doi: 10.82124/CEAS-GNC-2026-036 CEAS-GNC-2026-036

Automated Mixed-Sensitivity Design Based on Typical Launcher Performance Specifications

David Secades MSc, Aalborg University, Aalborg, Denmark. davidsc@es.aau.dk

Aitor Gomez PhD, Aalborg University, Aalborg, Denmark. arg@es.aau.dk

Paulo Rosa Head of the Avionics Business Unit, DEIMOS Engenharia SA, Lisbon , Portugal. paulo.rosa@deimos.com.pt

João Belfo GNC Engineer, DEIMOS Engenharia SA, GNC Competence Center, Lisbon , Portugal. joao.belfo@deimos.com.pt

Jakob Stoustrup Professor, Aalborg University, Aalborg, Denmark. jakob@es.aau.dk

ABSTRACT

Applications of H-infinity controller design as presented in the literature often rely significantly on manual tuning and iteration. This paper proposes uncertainty lumping, a novel framework which can increase the automation of the tuning process, simplify the weight design and reduce the conservativeness of the controller synthesis. Uncertainty lumping combines unstructured and parametric uncertainties while preserving their dependency relationships. This enables arbitrary combinations of competing and dependent requirements, along with system uncertainties, to be incorporated into the synthesis process. Furthermore, worst-case stability requirements can now be expressed as weights. To showcase the potential of this framework, the Thrust Vector Control (TVC) of a rigid-body launch vehicle is considered. A gain-scheduled robust controller is designed for the ascent phase. The applicable requirements from the VEGA rocket are translated into simple, well-known weights and lumped together into an equivalent weight that encodes the robust stability condition, as well as the stability requirements for nominal and worst-case conditions. The resulting controller is successfully validated against the ESA-i4GNC non-linear simulator and by frequency analysis, where the lumped weights are employed. The H-infinity norm of the synthesized controller is compared to that of the textbook approach, demonstrating reduced conservativeness.

Keywords: Robust control, GNC, uncertainty lumping, H-infinity weight design

Nomenclature

ψ, θ, ϕ	=	Euler angles (yaw, pitch, roll)
x, y, z	=	Drift from reference axis
$T(s)$	=	Complementary sensitivity
ω_B	=	Complementary sensitivity cut-off frequency
DM	=	Delay Margin
GLV	=	Generic Launch Vehicle

GM = Gain Margin
GNC = Guidance, Navigation, and Control
HF = High Frequency
LF = Low Frequency
LFT = Linear Fractional Transform
LPV = Linear Parameter-Varying
LTI = Linear Time-Invariant
LV = Launch vehicle
$MIMO$ = Multiple-Input Multiple-Output
PD = Proportional-Derivative
RS = Robust Stability
$SISO$ = Single-Input Single-Output
TVC = Thrust Vector Control

1 Introduction

One of the strengths of H_∞ control theory is its ability to encode stability and performance requirements into weights. These weights are supplied to the synthesis algorithm to automatically tune a controller that satisfies the requirements. However, as noted by Navarro [1, Sec. 3.4], "The selection of the weighting functions generally implies an iterative process with several heuristic steps to obtain an adequate set of weights." Therefore, it is often preferred in the literature to limit the use of frequency-dependent weights in favor of constant ones, which often encode a single requirement at a time [2, 3]. The trade-off is further manual tuning for a satisfactory design. This approach is viable for small-scale problems, but can quickly become impractical when the requirement set grows in size or complexity, as is the case in this paper's example.

Other approaches tailor weights, usually pole-zero pairs or low-pass filters, to encode certain requirements together [4–6]. The resulting weights offer greater tuning control, while their design is often unique to the specific set of requirements and lacks the flexibility to be generalized. Yet other approaches choose to employ more advanced theories like Linear Parameter-Varying Control (LPV) or μ-synthesis, with their associated complexity increase.

To address these challenges, this paper formalizes the solution developed in the main author's master thesis and proposes uncertainty lumping, a framework aimed at simplifying the weight design process while extending its capabilities. Uncertainty lumping seeks to reduce the complexity of expressing multiple requirements within a single weight by allowing simple weights, derived from well-known relationships, to be lumped together. Furthermore, the framework is designed to enable the encoding of worst-case stability requirements into a weight. Therefore, more information can be provided to the synthesis algorithm while reducing the required effort, which facilitates the automation of H_∞ controller design.

Finally, uncertainty lumping is applied to the Thrust Vector Control (TVC) of a rigid-body launch vehicle (LV) to showcase its application and benefits. The remainder of this paper is organized as follows: Section 2 describes the Generalized Launch Vehicle (GLV) model; Section 3 explains the selected requirements from the VEGA rocket; Section 4 defines uncertainty lumping and its advantages; Section 5 contains the controller design; Section 6 focuses on the validation of the synthesized controller.

2 Generic Launch Vehicle Model

In the context of this paper, a Generic Launch Vehicle (GLV) is a non-linear, rigid-body Launch Vehicle (LV) which satisfies the following assumptions:

- The roll ϕ is controlled by a separate system which bounds the roll rate $\dot{\phi}$ sufficiently low.
- The launch vehicle presents cylindrical symmetry on the pitch θ and yaw ψ axes.

Although LV flexible modes could be introduced into this analysis, they are not dominant in the problem considered here and are therefore omitted for clarity. The dynamics of the GLV pitch and yaw axes are linearized at 15 different time instants, uncoupled and represented by the same model [7 Sec 8.3; 8, Sec 3.3.2; 9, Sec 5.3.4.1]. The free body diagram of such a GLV pitch axis is shown in Figure 1.

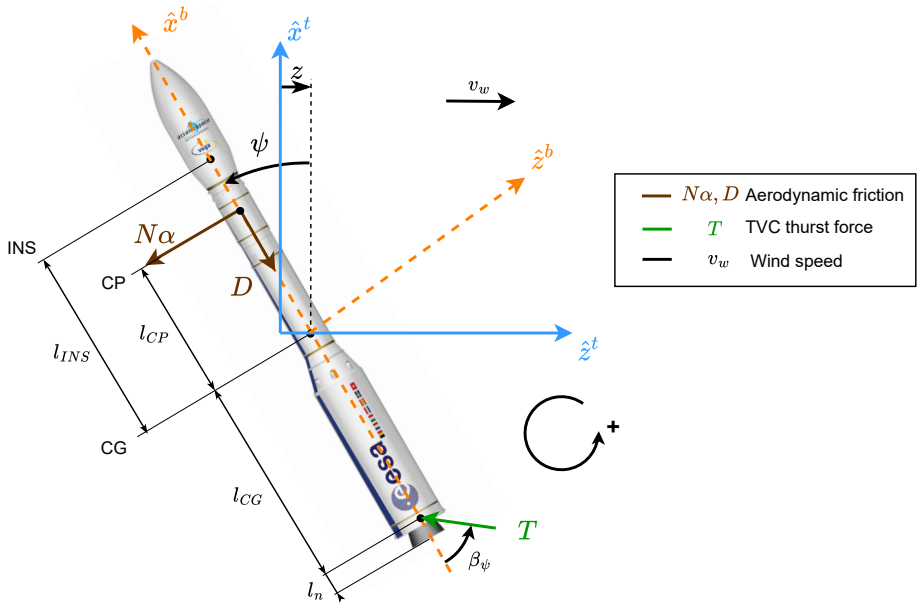

Fig. 1 Free body diagram of a GLV. Adapted from [1, Sec 2.2.1.1]

This GLV representation is expanded with a wind model $G_d(s)$ and a TVC model $G_{TVC}(s)$ containing uncertain dynamics $G_{LP}(s)$ and a constant delay $G_\tau(s)$. The resulting block diagram is depicted in Figure 2.

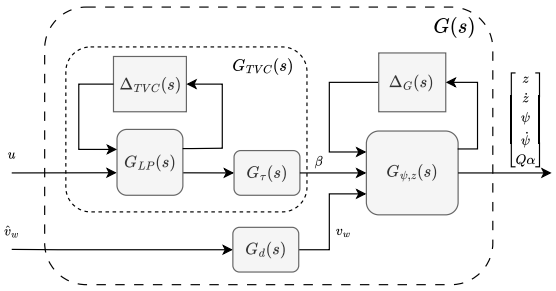

Fig. 2 Block diagram of the extended GLV model

2.1 $G_{\psi,z}(s)$ - Rigid-body dynamics

The uncoupled dynamics for each axis $G_{\psi,z}(s)$ represented in Figure 1 are transcribed into the state-space model of Eq. (1), which follows the form of [1, Sec 2.2.1.5;6, Sec 2.11]. The system inputs are the TVC actuator β and the wind speed disturbance v_w, while the states are the rotational and translational pair $\{\psi, z\}$ and their time derivatives. For this analysis, it is assumed that the states are available for

feedback. Finally, the dynamic pressure $Q\alpha$ is added as an output variable. The uncertainties associated to this model are specified in Table 2.

$$\begin{bmatrix} \dot{z} \\ \ddot{z} \\ \dot{\psi} \\ \ddot{\psi} \end{bmatrix} = \begin{bmatrix} 0 & 1 & 0 & 0 \\ 0 & \frac{-N}{V\,m} & \frac{D-T-N}{m} & \frac{l_{CP}N}{V\,m} \\ 0 & 0 & 0 & 1 \\ 0 & \frac{l_{CP}N}{V\,I_{yy}} & \frac{l_{CP}N}{I_{yy}} & \frac{-l_{CP}^2 N}{V\,I_{yy}} \end{bmatrix} \begin{bmatrix} z \\ \dot{z} \\ \psi \\ \dot{\psi} \end{bmatrix} + \begin{bmatrix} 0 & 0 \\ \frac{-T}{m} & \frac{N}{V\,m} \\ 0 & 0 \\ \frac{-l_{CG}T}{I_{yy}} & \frac{-l_{CP}N}{V\,I_{yy}} \end{bmatrix} \begin{bmatrix} \beta_\psi \\ v_w \end{bmatrix} \tag{1a}$$

$$\begin{bmatrix} z \\ \dot{z} \\ \psi \\ \dot{\psi} \\ Q\alpha \end{bmatrix} = \begin{bmatrix} 1 & 0 & 0 & 0 \\ 0 & 1 & 0 & 0 \\ 0 & 0 & 1 & 0 \\ 0 & 0 & 0 & 1 \\ -\frac{Q}{V} & 1 & 0 & Q \end{bmatrix} \begin{bmatrix} z \\ \dot{z} \\ \psi \\ \dot{\psi} \end{bmatrix} + \begin{bmatrix} 0 & 0 \\ 0 & 0 \\ 0 & 0 \\ 0 & 0 \\ 0 & -\frac{Q}{V} \end{bmatrix} \begin{bmatrix} \beta_\psi \\ v_w \end{bmatrix} \tag{1b}$$

2.2 $G_{TVC}(s)$ - TVC actuator model

The TVC actuator model $G_{TVC}(s)$ contains an uncertain second-order low-pass filter $G_{LP}(s)$ and a constant delay $G_\tau(s)$, represented in Eqs. (2-3) respectively [1, Sec 2.2.2.3]. The former's uncertainties are defined in Table 3, while the latter is modeled as a second-order Padé approximation [10, Sec 5.6.3].

$$G_{LP}(s) = \frac{\hat{\beta}(s)}{u(s)} = \left[\begin{array}{cc:c} 0 & 1 & 0 \\ -\omega_n^2 & -2\,\zeta\,\omega_n & \omega_n^2\,K_{TVC} \\ \hdashline 1 & 0 & 0 \end{array}\right] \tag{2}$$

$$G_\tau(s) = \frac{\beta(s)}{\hat{\beta}(s)} = \frac{s^2\,\tau^2 - 6\,s\,\tau + 12}{s^2\,\tau^2 + 6\,s\,\tau + 12} \tag{3}$$

2.3 $G_d(s)$ - Wind model

The wind disturbance $G_d(s)$ is represented by the second-order Dryden filter in Eq. (4), as it has been used in previous analysis [11, Eq. 9; 12, Sec 2.3.13.1]. The input $\hat{v}_w$ is a white-noise signal with root mean square σ_h, which represents the percentage of winds included in the analysis.

$$G_w(s) = \sigma_h \sqrt{\frac{V_t}{L_h}} \frac{\sqrt{\frac{3}{\pi}}s + \frac{V_t}{\sqrt{\pi}L_h}}{s^2 + 2\frac{V_t}{L_h}s + \left(\frac{V_t}{L_h}\right)^2} \tag{4}$$

where $V_t(t) = V(t) - v_{wp}(t)$ is the relative wind speed, $V(t)$ is the GLV airspeed and $v_{wp}(t)$ is the low-frequency wind profile. The turbulence scale L_h and σ_h depend on the selected altitude and turbulence level. Tabulated values can be found in [12, Tab 2.71].

2.4 $G(s)$ - Complete model

The GLV block diagram shown in Figure 2 represents each linearization point every 10 s from 10 to 150 s, yielding 15 linear time-invariant (LTI) state-space models. To showcase the approach proposed in this paper, a SISO plant is required. The channel $\beta_\psi \rightarrow \psi$ shown in Figure 3 is selected as it forgoes lateral control in favor of maintaining an accurate model of the angular dynamics[13].

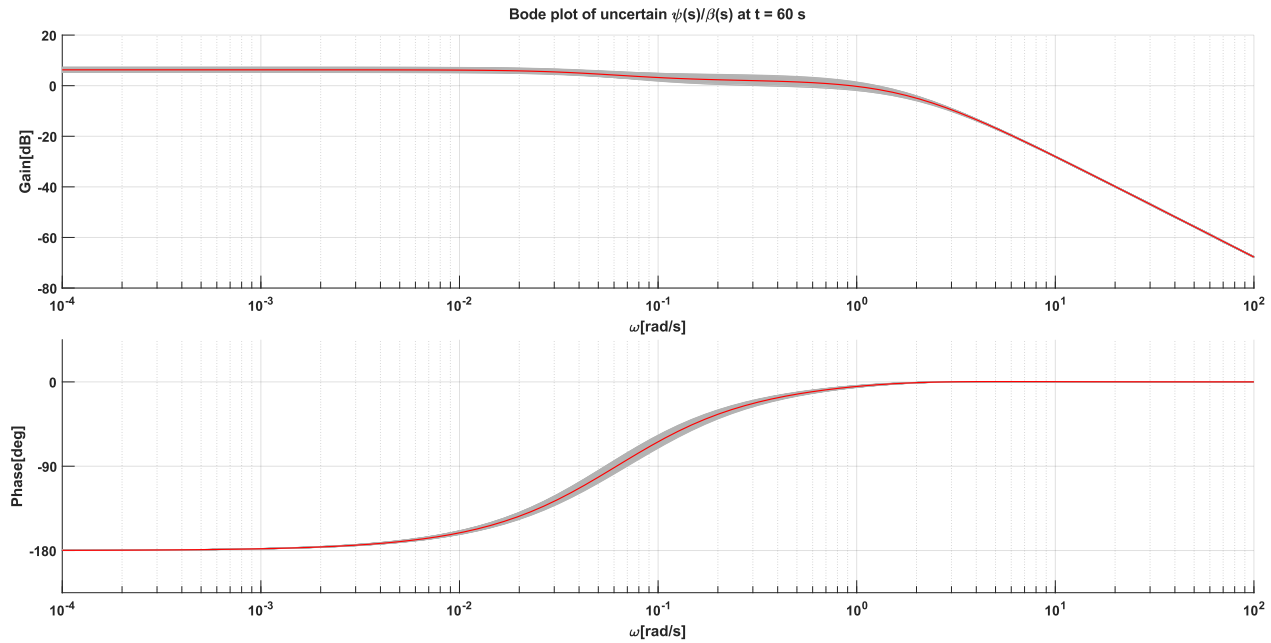

Fig. 3 Bode plot of $G_{\beta_\psi \to \psi}$ at worst Qα (t = 60 s) under nominal (red) and uncertain (grey) conditions

3 Requirements

Due to the lack of specific requirements for the available GLV model, the VEGA requirements shown in Table 1 have been chosen instead [1, Tab 2.1].

Table 1 Main VEGA requirements for TVC [1, Tab 2.1], filtered for a GLV

Requirements	Metrics		Bounds
Rigid-body stability margins	GM_{LF}	Nominal	≥ 6 dB
		Dispersed	≥ 0.5 dB
	DM	Nominal	≥ 100 ms
		Dispersed	≥ 40 ms
	GM_{HF}	Nominal	≤ -6 dB
		Dispersed	≤ -3 dB
Load Performance	Q_α		$< \bar{Q}_\alpha(t)$
Actuation Performance	β		6.5°
	Integrated angle		250 ° s
Pointing Performance	e_ψ		≤ 1 deg

The gain margins from Table 1 follow Eq. (5), while the delay margins follow Eq. (6). Both definitions are consistent with previous Guidance, Navication and Control (GNC) bibliography [1, Sec 2.1.5; 14, Sec F.1].

$$GM = |L(j\omega)|, \quad \forall \omega : \angle L(j\omega) = 180\,\text{deg} \tag{5}$$

$$DM = \frac{PM}{\omega_{PM}} \tag{6}$$

The maximum dynamic pressure bound $\bar{Q}_\alpha$ from Table 1 ensures the LV can resist the aerodynamic forces and survive launch. It can be seen in Figure 4, reproduced from Ref. [1, Fig 2.8].

The stability requirements from Table 1 define two different scenarios: nominal and dispersed conditions. The former must be satisfied by the nominal system, while the latter applies to the worst-case uncertainty. Encoding such requirements into weights is not common practice, and requires the *uncertainty lumping* approach proposed next in Section 4.

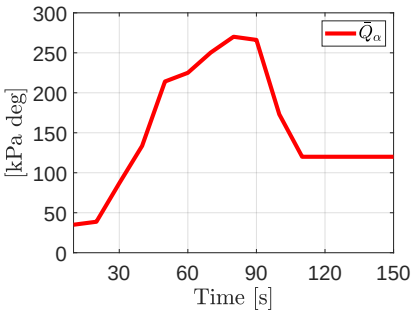

Fig. 4 Maximum dynamic pressure at each linearization point. Reproduced from[1, Fig 2.8]

4 Uncertainty lumping

The method described in this paper is henceforth referred to as *uncertainty lumping*, as it allows to unite unstructured uncertainties that bound the same transfer function into a single equivalent weight while maintaining the notion of independence, that is, whether each uncertainty must be satisfied in isolation (independent) or at the same time (dependent). As parametric uncertainties can be reinterpreted as unstructured uncertainties, uncertainty lumping allows to combine into a single weight both parametric and unstructured uncertainties, and by extension those requirements that can be represented by a frequency-dependent bound.

Sections 4.1 and 4.2 describe lumping of independent and dependent weights respectively, and their implications. Finally, Section 4.3 summarizes the uses and advantages of uncertainty lumping.

4.1 Case 1: Independent weights

Consider a set of n independent and competing requirements $r_i \ , \ \forall i \in \{1 \dots n\}$ for the same arbitrary transfer function $X(s)$ and their respective weight function $W_i(s)$. There requirements represent any property that can be transformed into a frequency bound, such as Gain Margin (GM), Delay Margin (DM) or cut-off frequency ω_B. For a SISO system, these conditions can be encoded in the controller synthesis via mixed-sensitivity synthesis [15, sec 2.8.3; 16, sec 5.7].

$$N(s) = \begin{bmatrix} \vdots \\ X(s)\, W_1(s) \\ \vdots \\ X(s)\, W_n(s) \end{bmatrix} \tag{7}$$

This paper proposes a simpler approach by noting

$$||N(s)||_{H_\infty} \ \leq \ \frac{1}{\sqrt{n}} \ \Rightarrow \ \left\{ \begin{array}{ll} |X(j\omega)\, W_1(j\omega)| \ \leq \ 1, & \forall\omega \\ \vdots & \\ |X(j\omega)\, W_n(j\omega)| \ \leq \ 1, & \forall\omega \end{array} \right\} \ \Leftrightarrow \ |X(j\omega)\, W_{eq}(j\omega)| \ \leq \ 1, \quad \forall\omega \tag{8}$$

where $||\cdot||_{H_\infty}$ represents the H_∞ norm of a transfer function [16, Sec 4.7], n represents the number of inequalities in the middle expression and $W_{eq}(s)$ is defined in Eq. (9), and lumps multiple weights

$W_i(s)$ into a single, equivalent one.

$$|W_{eq}| \;=\; \max(|W_1|, \ldots, |W_n|), \quad \forall\omega \tag{9}$$

As shown in Eq. (10), the relationship between the left and middle inequalities of Eq. (8) is only a necessary condition because, by definition, the region spanned by the left inequality is contained but not equal to the region of the middle expression. On the other hand, the relationship between the middle and right inequalities is a sufficient condition because the middle and right regions are equal. Therefore, the textbook approach increases conservativeness in the sense of a higher H_∞ norm for the same set of requirements, while the uncertainty lumping approach does not.

$$D_{left} \subsetneq D_{center} = \bigcup_{i=1}^{n} D_i \qquad \text{where } D_{right} \text{ represents the domain of expression } i \tag{10}$$

In conclusion, uncertainty lumping enables stacking multiple competing, independent requirements into a single weight $W_{eq}(s)$ through Eq. (9), hereafter referred to as Case 1, without increasing conservativeness.

4.2 Case 2: Uncertainty and worst-case requirements

Equation (8) also implies that, for a SISO system with multiplicative uncertainty bounded by $W_\Delta(s)$ and a set of requirements represented by the weight $W_T(s)$ for $T(s)$, the following holds:

$$\left.\begin{array}{rll} \text{RS} & \Leftrightarrow |T(j\omega)\,W_\Delta(j\omega)| \le 1, & \forall\omega \\ \text{Stability requirement} & \Leftrightarrow |T(j\omega)\,W_T(j\omega)| \le 1, & \forall\omega \end{array}\right\} \Leftrightarrow |T(j\omega)\,W_{eq}(j\omega)| \le 1, \quad \forall\omega \tag{11}$$

Where $W_{eq}(s)$ is lumped with Case 1. Notice that the RS condition and the stability requirement from Eq. (11) depend identically on a weight $W(s)$. This implies the RS problem is identical to the stability requirement problem with the same weight. In other words, a weight $W(s)$ on $T(s)$ can be interpreted as both a multiplicative uncertainty bound $W_\Delta(s)$ and a stability requirement weight $W_T(s)$, as the problems are equivalent. This is indeed a well-known property in the literature and will exploited next [15, Sec 7.5.2].

Consider an uncertain SISO system $G_p(s)$ with uncertainty bounded by a multiplicative weight $W_\Delta(s)$, and a set of requirements for the worst-case complementary sensitivity $T_{wc}(s)$ lumped in $W_{T,wc}(s)$ with Case 1. $W_{T,wc}(s)$ can be understood as another multiplicative uncertainty, which yields the equivalent block diagram depicted in Figure 5.

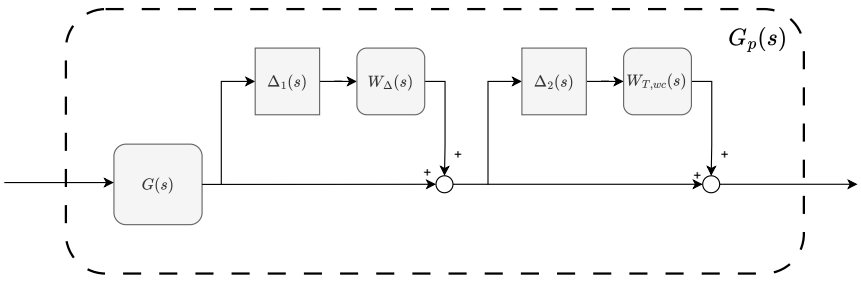

Fig. 5 Multiplicative uncertainty chain block diagram

$$G_p(s) \;=\; \big(1 + \Delta_2(s)W_{T,wc}(s)\big)\,\big(1 + \Delta_1(s)W_\Delta(s)\big)\,G(s); \quad ||\Delta_i(j\,\omega)||_{H_\infty} \le 1 \quad \forall\omega\,,\; i = 1,2 \tag{12}$$

This chain of uncertainties satisfies Eq. (12) and can be bounded from above by Eq. (13), where $W_{eq,wc}(s)$ is defined in Eq. (14), hereafter referred to as Case 2.

$$|G_p(j\omega)| \;\le\; |G(j\omega)(1 + \Delta_3(j\omega)\,W_{eq,wc}(j\omega))|; \quad |\Delta_3(j\,\omega)| \le 1 \quad \forall\omega \tag{13}$$

Equation (13) becomes tight for those $\Delta_1(s)$, $\Delta_2(s)$ that satisfy Eq. (15).

$$|W_{eq,wc}(j\omega)| = |W_\Delta(j\omega)| + |W_{T,wc}(j\omega)| + |W_\Delta(j\omega)||W_{T,wc}(j\omega)|, \quad \forall\omega \tag{14}$$

$$\angle(W_\Delta(j\omega)\,\Delta_1(j\omega)) = \angle(W_{T,wc}(j\omega)\,\Delta_2(j\omega) = 0, \quad \forall\omega \tag{15}$$

Because the weight $W_{eq,wc}(s)$ is tight for Eq. (13), the first inequality of Eq. (16) is a sufficient condition for both RS and satisfying the worst-case stability requirements encoded in $W_{T,wc}(s)$.

$$|T(j\omega)\,W_{eq,wc}(j\omega)| \leq 1, \quad \forall\omega \;\Leftrightarrow\; \begin{cases} |T(j\omega)\,W_\Delta(j\omega)| & \leq 1, \quad \forall\omega \\ |T(j\omega)\,W_{T,wc}(j\omega)| & \leq 1, \quad \forall\omega \end{cases} \tag{16}$$

Therefore, uncertainty lumping can be employed to generate a single weight that encodes both RS and a set of requirements for the worst-case complementary sensitivity, which is not possible with the current textbook approach. Now, worst-case stability requirements can be introduced into the synthesis process without increasing conservativeness.

4.3 Summary

By applying uncertainty lumping:

- expressing multiple independent, competing requirements for the same transfer function becomes straightforward with Case 1, as it is no longer required to derive separate weight expressions for each combination of requirements.
- it is now possible to encode worst-case stability requirements into the controller synthesis process with Case 2, which reduces the manual tuning required by providing the synthesis algorithm with more information.
- all nominal and worst-case stability requirements that can be encoded into frequency bounds, as well as uncertainty weights, can be combined into a single weight with appropriate use of Case 1 and Case 2 by matching their dependency relationships.
- the set of controllers produced by the synthesis algorithm more closely approximates the true set of controllers that satisfy the requirements, reducing conservativeness without increasing computational cost.

Uncertainty lumping has the potential to reduce manual tuning by including worst-case and/or competing requirements into the synthesis algorithm, while using a small set of rules that are easy to learn and to apply, while offering no drawbacks.

5 Controller Design

A block diagram of the chosen architecture is depicted in Figure 6. All inputs and outputs have been normalized and use the " $\hat{x}$ " notation. The system to control, $G(s)$, is represented in Figure 2, where the uncertainty blocks have been combined and pulled out. The chosen controller K is an ideal PD with input ψ, although in this design exercise it is represented as the partial state feedback shown in Figure 6. As $G(s)$ is linearized at the 15 different time instants defined before, the controller K is synthesized at each point and gain-scheduled.

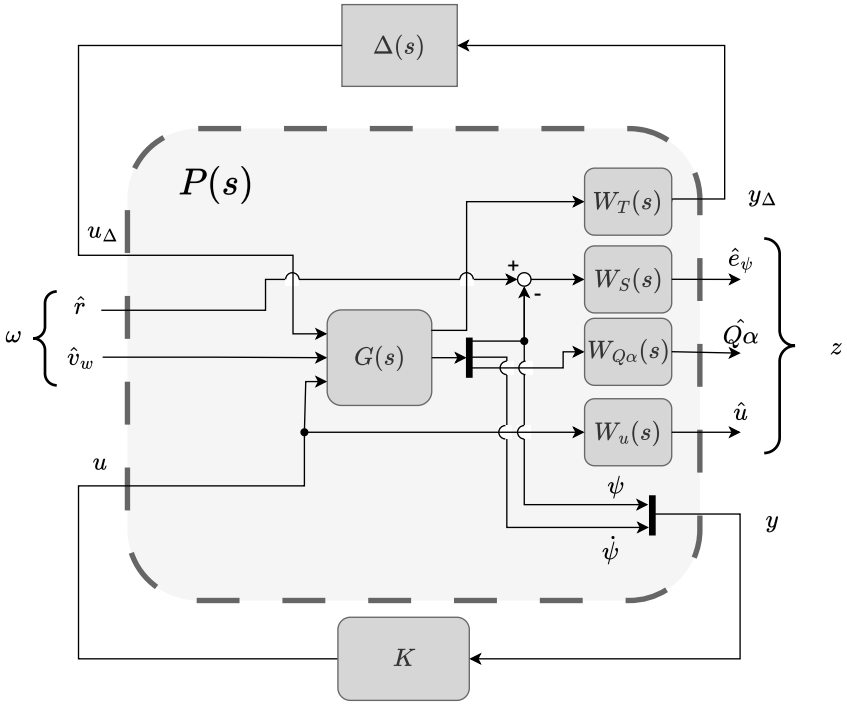

Fig. 6 Block diagram of the generalized plant P

All the frequency-dependent weights computed in this paper are shaped like the biproper weight $W(s)$ from Eq. (17) or a combination thereof, unless otherwise specified.

$$W(s) = \frac{s/M + w_B}{s + w_B A} \Leftrightarrow \begin{cases} \lim_{s\to 0} W(s)^{-1} = A \\ \lim_{s\to\infty} W(s)^{-1} = M \\ |W(j\,\omega_c)^{-1}| = 1, \quad \omega_c \approx w_B \end{cases} \tag{17}$$

5.1 $W_T(s)$ - Uncertainty and stability weight

First, the system uncertainty is modeled as a single multiplicative uncertainty $\{\Delta, W_\Delta\}_{t_i}$ for each linearization point t_i from Eq. (18) [15, Sec 7.4.4]. The resulting weights $W_\Delta(s)$ are plotted in Figure 7.

$$|W_\Delta| \;\geq\; l_w, \;=\; \forall\omega; \quad l_w(j\,\omega) \max_{G_p} \left| \frac{G_p(j\,\omega) - G(j\,\omega)}{G(j\,\omega)} \right| \tag{18}$$

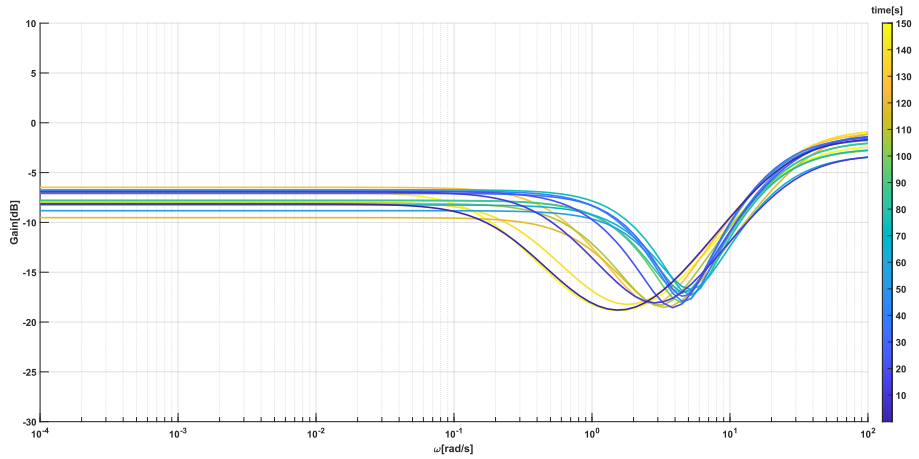

Fig. 7 Multiplicative uncertain weight $W_\Delta(s)$ with respect to the linearization point

The nominal and dispersed stability requirements are encoded into $W_{T,n}(s)$ and $W_{T,wc}(s)$ respectively. These weights are computed with the same method and, like the requirements, are independent from the linearization point t_i.

The gain margins GM_{LF} and GM_{HF} bound M_T from above [15, Sec 2.4.3], as shown in Eq. (19). Therefore, they can be encoded in a weight W_{GM} with $A = \{M_T\}_{LF}$, $M = \{M_T\}_{HF}$. Meanwhile, $w_B = \{10\,\text{rad/s}\}$ is chosen to satisfy $\omega_{GM_{HF}} >> \omega_B >> \omega_{GM_{LF}}$ to prevent distortion of $|W_{GM}(s)|$ at the GM frequencies.

$$\begin{cases} M_T \geq \frac{GM}{1-GM} & \text{if} \quad GM < 1 \\ M_T \geq \frac{GM}{GM-1} & \text{if} \quad GM > 1 \end{cases} \tag{19}$$

The delay margin can be encoded into a multiplicative uncertainty weight $W_{DM}(s)$ with Eq. (18) by reinterpreting it as an uncertain delay [15, Sec 7.4.5]. These requirements $W_{GM}(s)$ and $W_{DM}(s)$ are independent and can be lumped together with Case 1. The resulting weights for nominal $W_{T,n}(s)$ and dispersed $W_{T,wc}(s)$ conditions are represented in Figure 8.

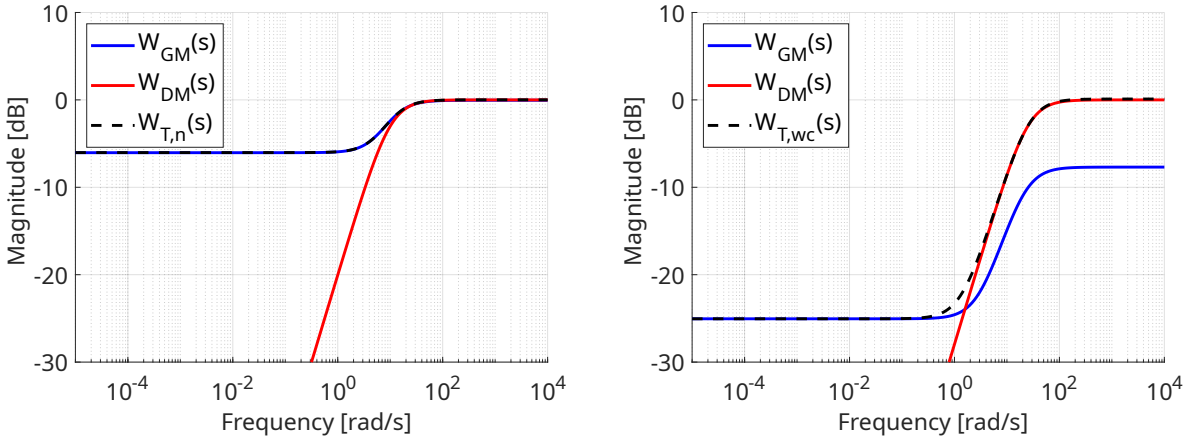

(a) Nominal **(b) Disperse**

Fig. 8 Stability requirement weights under nominal and dispersed conditions

The dispersed requirements $W_{T,wc}(s)$ must be satisfied at the worst-case uncertainty encoded in $W_\Delta(s)$, which makes them dependent. These are lumped together through Case 2 into a weight which

represents the dispersed conditions. These dispersed conditions are independent of the nominal conditions encoded in $W_{T,n}(s)$ as they define different situations, so they are lumped into the final equivalent weight $W_T(s)$ through Case 1. The bound imposed by $W_T(s)$ is now a sufficient condition for RS, for satisfying the nominal requirements and for satisfying the dispersed requirements. Once again, the pertinent weights are plotted in Figure 9.

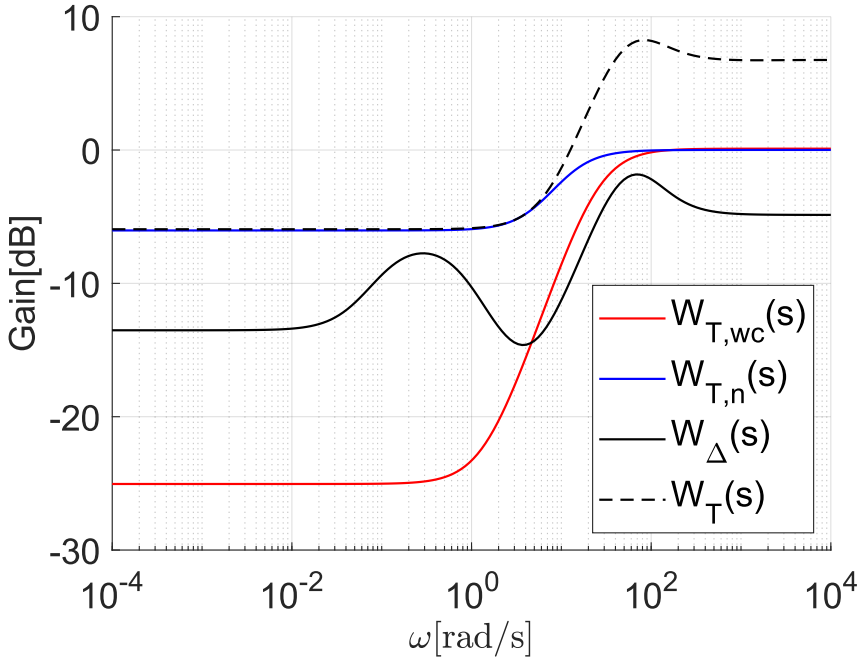

Fig. 9 Lumped weight $W_T(s)$ for uncertainties and stability requirements at worst $Q\alpha$ ($t = 60$ s)

5.2 $W_S(s)$ - Pointing error weight

The pointing error requirement $\bar{e}_\psi$ is encoded to $W_S(s)$ in Eq. (20) . The cut-off frequency was chosen to satisfy $w_B << 10$ rad/s to only affect the synthesis at low frequencies.

$$W_S(s) = \frac{s/100 + 1}{s + \bar{e}_\psi} \tag{20}$$

5.3 $W_{Q\alpha}(s)$ - Dynamic pressure weight

The maximum dynamic pressure at each linearization point is represented in Figure 4. There is no extra requirements for this signal, although this weight does depend on the linearization point, and thus varies for each synthesis.

$$W_{Q\alpha}(s) = \left(\bar{Q}_\alpha\right)^{-1} \tag{21}$$

5.4 $W_u(s)$ - Actuator effort weight

The maximum actuator effort requirement $\bar{u}$ is encoded identically to $\bar{Q}_\alpha$. The second requirement bounds the integral of u, and is thus represented by its Laplace transform s^{-1} as shown in Eq. (22).

$$W_{u,r1}(s) = (\bar{u})^{-1} \quad , \quad W_{u,r2}(s) = \left(\frac{\bar{u}_{int}}{s}\right)^{-1} \tag{22}$$

These weights represent independent requirements and are lumped through Case 1 into $W_u(s)$ as depicted in Figure 10.

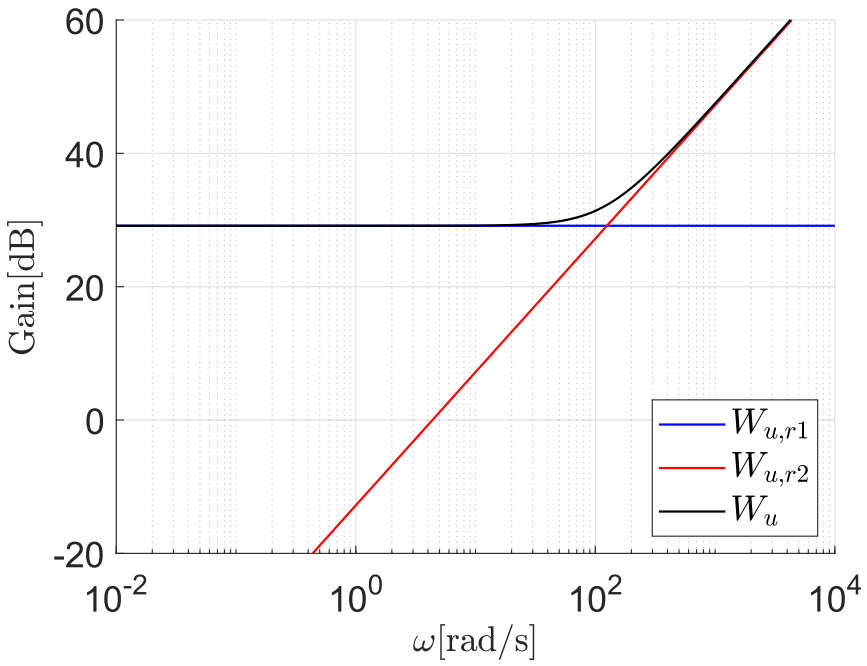

Fig. 10 Lumped weight $W_u(s)$ for actuator effort.

5.5 Synthesis problem

The synthesis objective function $N_m(s) = F_\ell(P, K)$ is MIMO. To convert back to a SISO problem, only one exogenous input ω must be considered for each exogenous output z and for y_Δ. The chosen channels and final objective function $N(s)$ are:

$$\begin{bmatrix} y_\Delta \\ e_\psi \\ u \\ Q\alpha \end{bmatrix} = N_m(s) \begin{bmatrix} u_\Delta \\ r_\psi \\ \hat{v}_w \end{bmatrix} \quad , \quad N_m(s) = \begin{bmatrix} W_T(s)\,T(s) & 0 & 0 \\ 0 & W_S(s)\,S(s) & 0 \\ 0 & 0 & W_U(s)\,K(s)\,S(s) \\ 0 & 0 & W_{Q\alpha}(s) G_{Q\alpha}(s) \end{bmatrix} \tag{23}$$

$$N(s) = \begin{bmatrix} W_T(s)\,T(s) \\ W_S(s)\,S(s) \\ W_U(s)\,K(s)\,S(s) \\ W_{Q\alpha}(s)\,G_{Q\alpha}(s) \end{bmatrix} \tag{24}$$

The objective function $N(s)$ is used to synthesize a controller K at each linearization point with hinfstruct()[1].

[1] See `https://www.mathworks.com/help/robust/ref/dynamicsystem.hinfstruct.html`

6 Results

6.1 Frequency analysis

The controller has been synthesized, and the resulting H_∞ norms can be seen in Figure 11a, except the RP condition which is shown in Figure 11b. Every norm is smaller than one, therefore the synthesized controller satisfies the requirements. The lumped weights $W_T(s)$ and $W_U(s)$ are shown instead of the H_∞ norm associated to each requirement, as satisfying the former is equivalent to the latter. Experienced readers may notice no norm reaches unity. Therefore, the requirements may be tightened to obtain further performance.

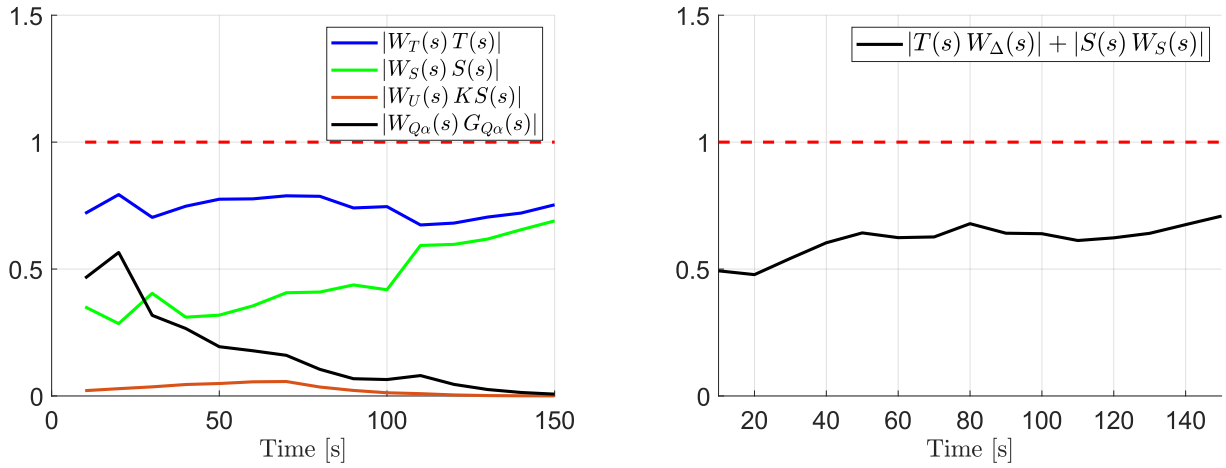

(a) Element-wise H_∞ norm of minimized objective function $N(s)$

(b) H_∞ norm of the robust performance condition

Fig. 11 Frequency analysis results: H_∞ norms

To prove the weight $W_T(s)$ correctly encodes the RS condition as well as the nominal and dispersed stability requirements, the Nichols plot of the uncertain loop transfer function $L(s) = G(s)\,K(s)$ is shown in Figure 12. The system is robustly stable, as none of the uncertain systems cross the -1 point. Moreover, neither the nominal (red) nor the uncertain (grey) systems enter their respectively colored triangular dashed regions, thereby satisfying the stability requirements.

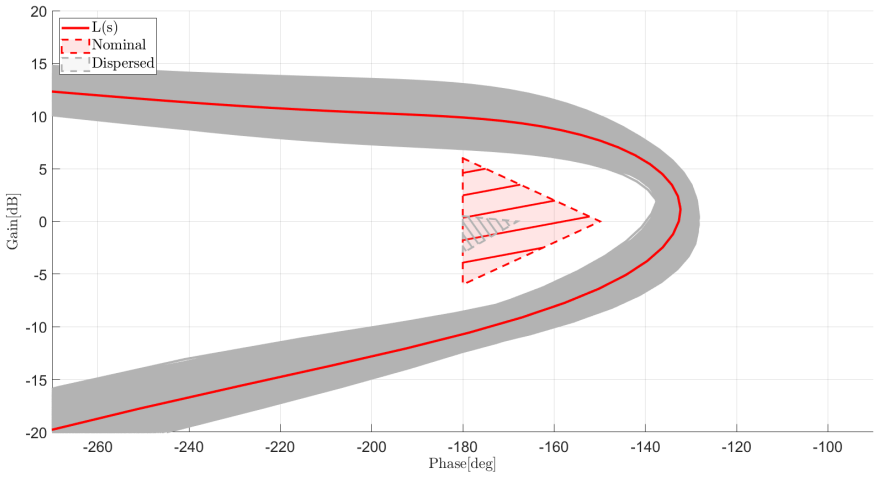

Fig. 12 Nichols plot of $G(s)K(s)$ for nominal (red) and dispersed (grey) conditions, with corresponding stability constraints shown as triangular regions

Figure 13 seen below compares the H_∞ norm of the minimized $N(s)$ obtained in this paper through uncertainty lumping, versus the equivalent H_∞ norm without it. As such, $N_{non-lumped}(s)$ is computed with the same controller $K(s)$ and the weights $W_{GM}(s)$, $W_{DM}(s)$, $W_\Delta(s)$, $W_S(s)$, $W_{Q\alpha}(s)$, $W_{u,r1}(s)$, $W_{u,r2}(s)$ stacked with their respective transfer functions. This paper's method shows a smaller H_∞ norm for the same controller, and is therefore less conservative.

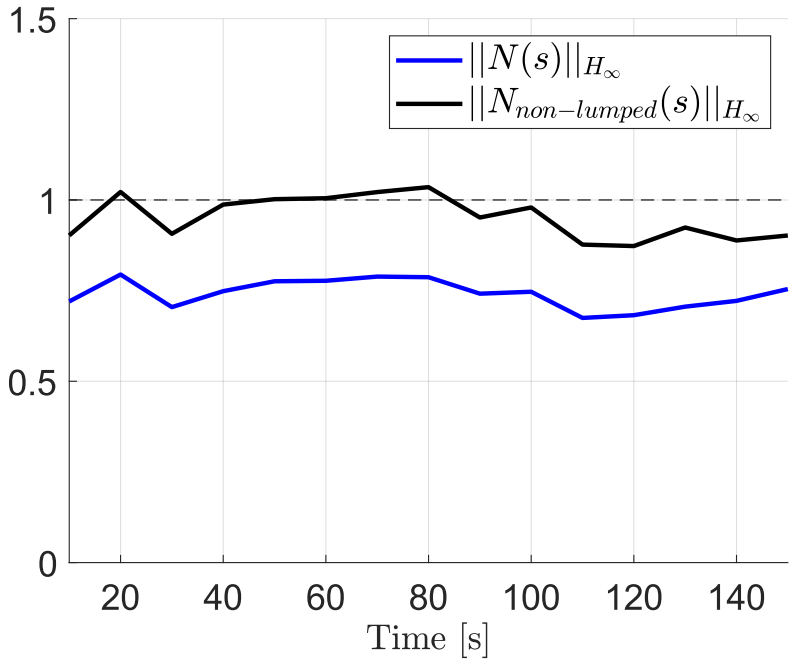

Fig. 13 Conservativeness comparison: H_∞ norm of $N(s)$ vs $N_{non-lumped}(s)$ for the same closed-loop system

6.2 V&V Campaign

Although this paper focuses on the advantages of uncertainty lumping for automating the controller synthesis, the controller is still validated in the ESA-i4GNC non-linear simulator as similar papers for

completeness[5, 14]. In this simulation, a gravity turn maneuver is employed as the reference, with realistic wind disturbances of moderate level as defined in [12, Tab 2.71]. A total of 30 Monte Carlo runs are executed with the uncertainties from Tables 2–3. The pertinent plots can be found in Appendix 7.

The results show a satisfactory design, validating the controller obtained with uncertainty lumping. The pointing error lies within 2 deg. The dynamic pressure and actuator effort requirements are also satisfied with a high margin, which was previously predicted in our frequency analysis and is caused by the requirements set belonging to a different LV.

7 Conclusions

In this paper a new weight design approach based on uncertainty lumping is proposed. An H_∞ robust, time-scheduled PD controller is designed for the TVC of a generic launch vehicle (GLV) during the ascent phase. A set of stability and performance requirements are adapted from the VEGA rocket. These requirements differentiate between nominal and worst-case stability bounds and are specifically selected to showcase uncertainty lumping.

The textbook approach cannot handle this distinction directly, as it requires one set of conditions to be selected for controller synthesis while the other must be verified afterwards manually. In contrast, uncertainty lumping allows each requirement to be encoded first into its well-known frequency bound, which is then reinterpreted as a parametric uncertainty. These uncertainties are subsequently lumped together with other structured and/or unstructured uncertainties into a single equivalent weight.

This process relies on only two cases, which are independent of the specific set of requirements, do not scale in complexity or conservativeness with respect to size, and are simple to automate. From a design perspective, uncertainty lumping reduces the manual tuning required to obtain a suitable controller. It does so by increasing the number of requirements that can be supplied to the synthesis algorithm while automating their translation into weights, making it a valuable tool for control design engineers.

To demonstrate the effectiveness of uncertainty lumping, the resulting controller is validated through frequency analysis methods and against the ESA-i4GNC non-linear simulator. All design specifications are satisfied in a highly simplified design process.

The proposed method applies to any SISO system. While it enables automation of frequency-domain requirements, time-domain specifications still require manual tuning if no equivalent frequency-bound is available. The approach also generalizes to MIMO systems, although the lumping process may introduce conservativeness and cross-dependencies that warrant further study.

Appendix

Uncertainty tables

The uncertainties considered for the design and V&V campaign are shown in Tables 2–3.

Table 2 Model time-independent parametric uncertainties

Parameter	Description	Uncertainty[%]
D	Aerodynamic drag force	5
N	Aerodynamic lateral force	15
I_{yy}	Pitch axis inertia	2
Q	Dynamic pressure	15
T	TVC thrust force	0.1
V	Non-gravitational speed	5
l_{cog}	Distance from CoG to TVC	5
l_{cp}	Distance from CoG to CoP	2

Table 3 Actuator time-independent parametric uncertainties

Parameter	Description	Uncertainty[%]
ω_n	Actuator bandwidth	20
K_{TVC}	DC gain	10
ζ	Damping ratio	28.5

Monte Carlo simulation results

The resulting graphs of the V&V campaign can be seen next:

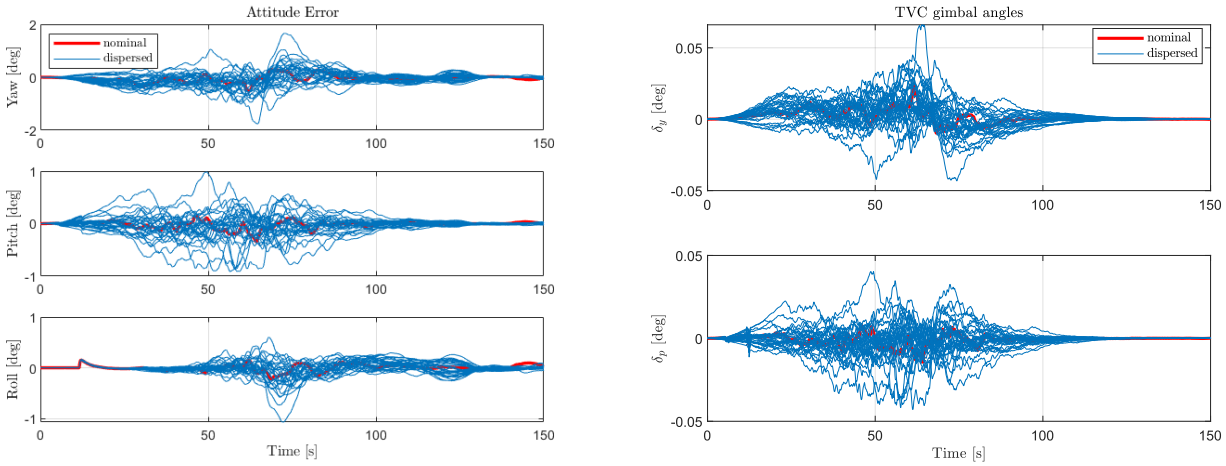

(a) Pointing error with respect to reference **(b) TVC actuator effort**

Fig. 14 Reference tracking results of V&V campaign during gravity-turn maneuver

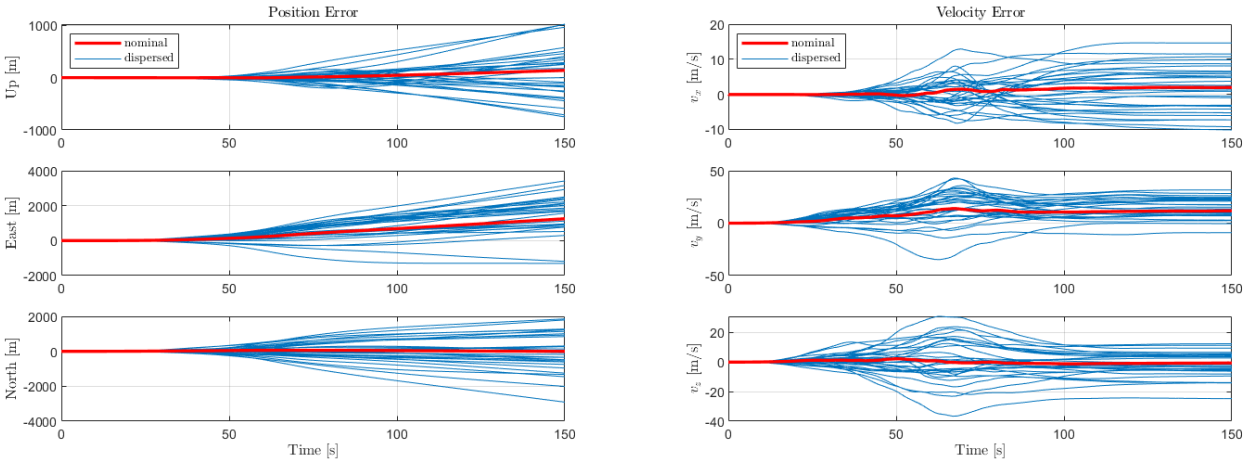

(a) Drift **(b) Drift speed**

Fig. 15 Lateral control results of V&V campaign

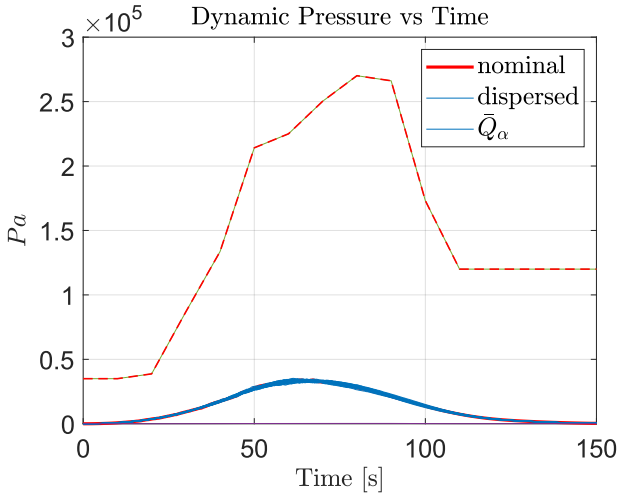

Fig. 16 Dynamic pressure of V&V campaign

Acknowledgments

The authors of this paper want to thank specifically INDRA-DEIMOS for providing the Linear Functional Transform (LFT) data and ESA-i4GNC non-linear simulator that made this paper possible.

Declaration of Use of Artificial Intelligence

Artificial intelligence was employed to identify grammatical mistakes and more accurate vocabulary. All proposed changes were carefully considered by the author before implementation. Other peers have proofread this paper. Outside of this case, artificial intelligence was not used in the work presented.

References

[1] Diego Navarro-Tapia. *Robust and Adaptive TVC Control Design Approaches for the VEGA Launcher*. PhD thesis, University of Bristol, Bristol,United Kingdom, June 2019. https://research-information.bris.ac.uk/en/studentTheses/robust-and-adaptive-tvc-control-design-approaches-for-the-vega-la.

[2] Andrei F. Cojocaru, Alexandru Lapusneanu, and Paulo Rosa. Application of a Mixed H2/H-infinity Synthesis Approach to the Control Problem of the LISA Mission. In *Proceedings of the 2024 CEAS Specialist Conference on Guidance, Navigation and Control (EuroGNC)*, Bristol, UK, Dec. 2024. doi: 10.82124/CEAS-GNC-2024-098.

[3] Abdelmoez Elagroudy, Christian Weiser, Simon Schulz, and Jan Tilmans. Flight Control Law Design using H-inifinity optimal control for Gust Load Alleviation of Flexible Aircraft. In *Proceedings of the 2024 CEAS Specialist Conference on Guidance, Navigation and Control (EuroGNC)*, Bristol, UK, Dec. 2024. doi: 10.82124/CEAS-GNC-2024-040.

[4] Mohamad Hachem, Clément Roos, and Thierry Miquel. Application of Reduced-Order Robust Control to Multi-Rotor Stabilization and Guidance. In *Proceedings of the 2024 CEAS Specialist Conference on Guidance, Navigation and Control (EuroGNC)*, Bristol, UK, Dec. 2024. doi: 10.82124/CEAS-GNC-2024-055.

[5] João Belfo, Nicola Somma, Alejandro Montero, Paulo Rosa, João Santos, Tiago Moreira, Pedro Simplício, António Rinalducci, and Yohann Torres. Robust Control Design for a Sub-Orbital Launch Vehicle with Destabilizing Sloshing Dynamics. In *Proceedings of the 2024 CEAS Specialist Conference on Guidance, Navigation and Control (EuroGNC)*, Bristol, UK, Dec. 2024. doi: 10.82124/CEAS-GNC-2024-044.

[6] Ricardo Rodrigues, Francesco Sanfedino, and Daniel Alazard. Linear Parameter-Varying gain-scheduled attitude controller for a spinning spacecraft involving large flexible booms. In *Proceedings of the 2024 CEAS Specialist Conference on Guidance, Navigation and Control (EuroGNC)*, Bristol, UK, Dec. 2024. doi: 10.82124/CEAS-GNC-2024-008.

[7] Pedro V. Simplício. *Guidance and Control Elements for Improved Access to Space*. PhD thesis, University of Bristol, Bristol,United Kingdom, Nov. 2019. https://research-information.bris.ac.uk/en/studentTheses/guidance-and-control-elements-for-improved-access-to-space/.

[8] Bong Wie and Wei Du. Analysis and Design of Launch Vehicle Flight Control Systems. In *AIAA Guidance, Navigation & Control Conference & Exhibit*, Honolulu, Hawaii, Aug. 2008. doi: https://doi.org/10.2514/6.2008-6291.

[9] David Sánchez. *Design of H-Infinity controllers for ill-conditioned plants in presence of disturbances*. PhD thesis, Complutense University of Madrid (UCM), Madrid, Spain, May 2015. https://produccioncientifica.ucm.es/documentos/5f63fc8629995274fc8e8377.

[10] Gene F. Franklin, J. David Powell, and Emami-NaeinimAbbas. *Feedback Control of Dynamic Systems 8th editions*. Pearson, 2020. ISBN: 978-1-292-27452-2.

[11] Michael M. Madden. Verifying Implementation of the Dryden Turbulence Model and MIL-F-8785 Gust Gradient. Atlanta, GA, USA, June 2018. AIAA. doi: 10.2514/6.2018-3580.

[12] D. L. Johnson. *Terrestrial Environment (Climatic) Criteria Guidelines for use in Aerospace Vehicle Development*. Marshall Space Flight Center, Alabama, USA, Dec. 2008. ISBN: 978-1-62410-302-5.

[13] F. O. Ramos, Leite Filho W. C., and F. J. O. Moreira. Gain computation strategy for an attitude control system. In *17th International Congress of Mechanical Engineering*, SP, Brazil, Nov. 2003. https://www.abcm.org.br/anais/cobem/2003/html/pdf/COB03-0620.pdf.

[14] Pedro Simplício, Samir Bennani, Xavier Lefort, Andrés Marcos, and Christophe Roux. Structured Singular Value Analysis of the VEGA Launcher in Atmospheric Flight. *Journal of Guidance, Control, and Dynamics*, 39(6), Mar 2016. doi: 10.2514/1.G000335.

[15] Sigurd Skogestad and Ian Postlethwaite. *Multivariate Feedback Control: Analysis and Design*. John Wiley & Sons Ltd, 2006. ISBN: 978-0-470-01167-6.

[16] Kemin Zhou, John C. Doyle, and Keith Glover. *Robust and Optimal Control*. Prentice Hall, 1996. ISBN: 978-0134565675.